Supporting Information

Electronic Engineering of Amorphous Fe-Co-S sites in Hetero-nanoframes For Oxygen Evolution and Flexible Al-air Batteries

Min Lu[a], Li An[a], Jie Yin[a], Jing Jin[a], Rui Yang[a], Bolong Huang,*[b] Yang Hu[a], Yong-Qing Zhao[a], and Pinxian Xi,*[a]

[a] State Key Laboratory of Applied Organic Chemistry, Frontiers Science Center for Rare Isotopes, College of Chemistry and Chemical Engineering, Lanzhou University, Lanzhou 730000, China. E-mail: xipx@lzu.edu.cn
[b] Department of Applied Biology and Chemical Technology, The Hong Kong Polytechnic University, Hung Hum, Kowloon, Hong Kong SAR, China. E-mail: bhuang@polyu.edu.hk

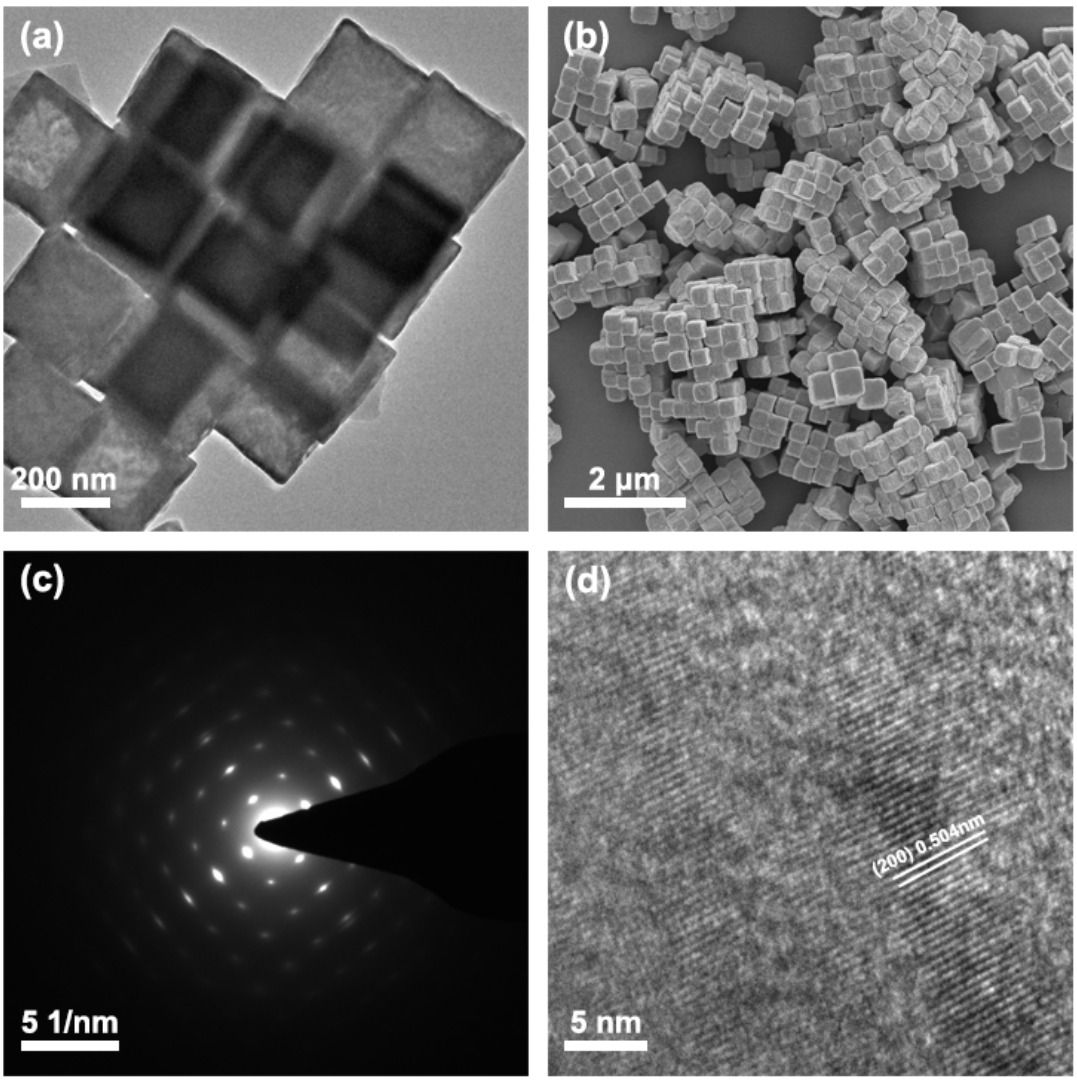

Figure S1. (a) TEM image of PBA. (b) SEM image of PBA. (c) SAED image of PBA. (d) HRTEM image of PBA.

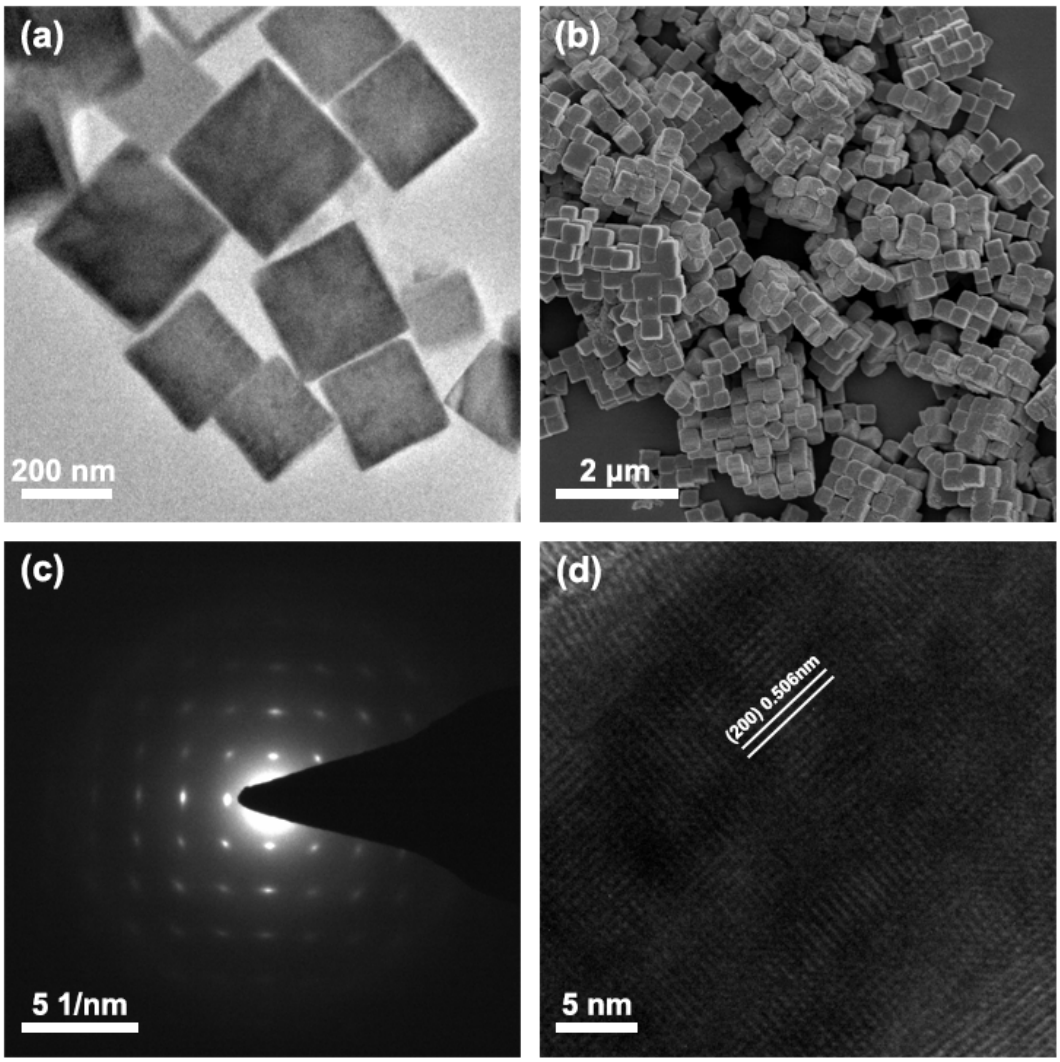

Figure S2. (a) TEM image of MPBA. (b) SEM image of MPBA. (c) SAED image of MPBA. (d) HRTEM image of MPBA.

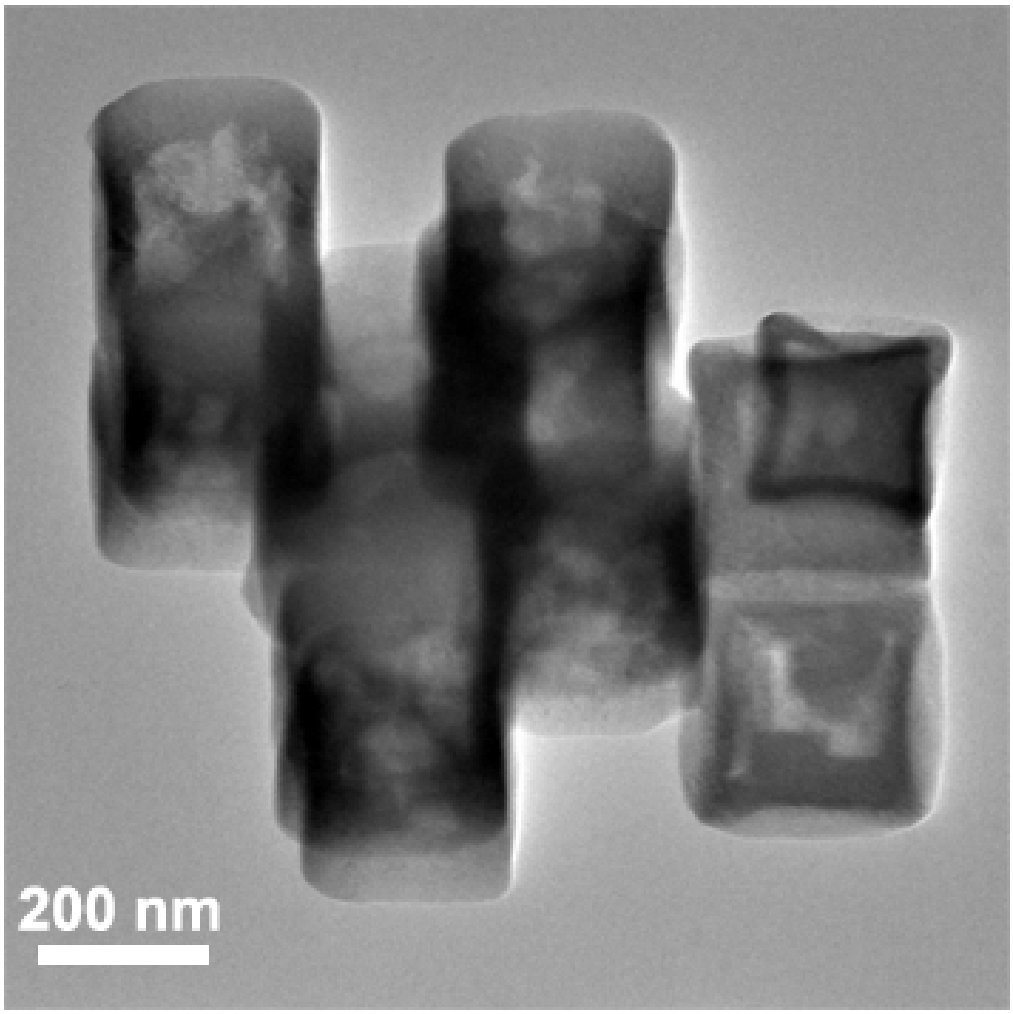

Figure S3. TEM image of PBA corroded by 2 M HCl without the exist of Fe^{2+}.

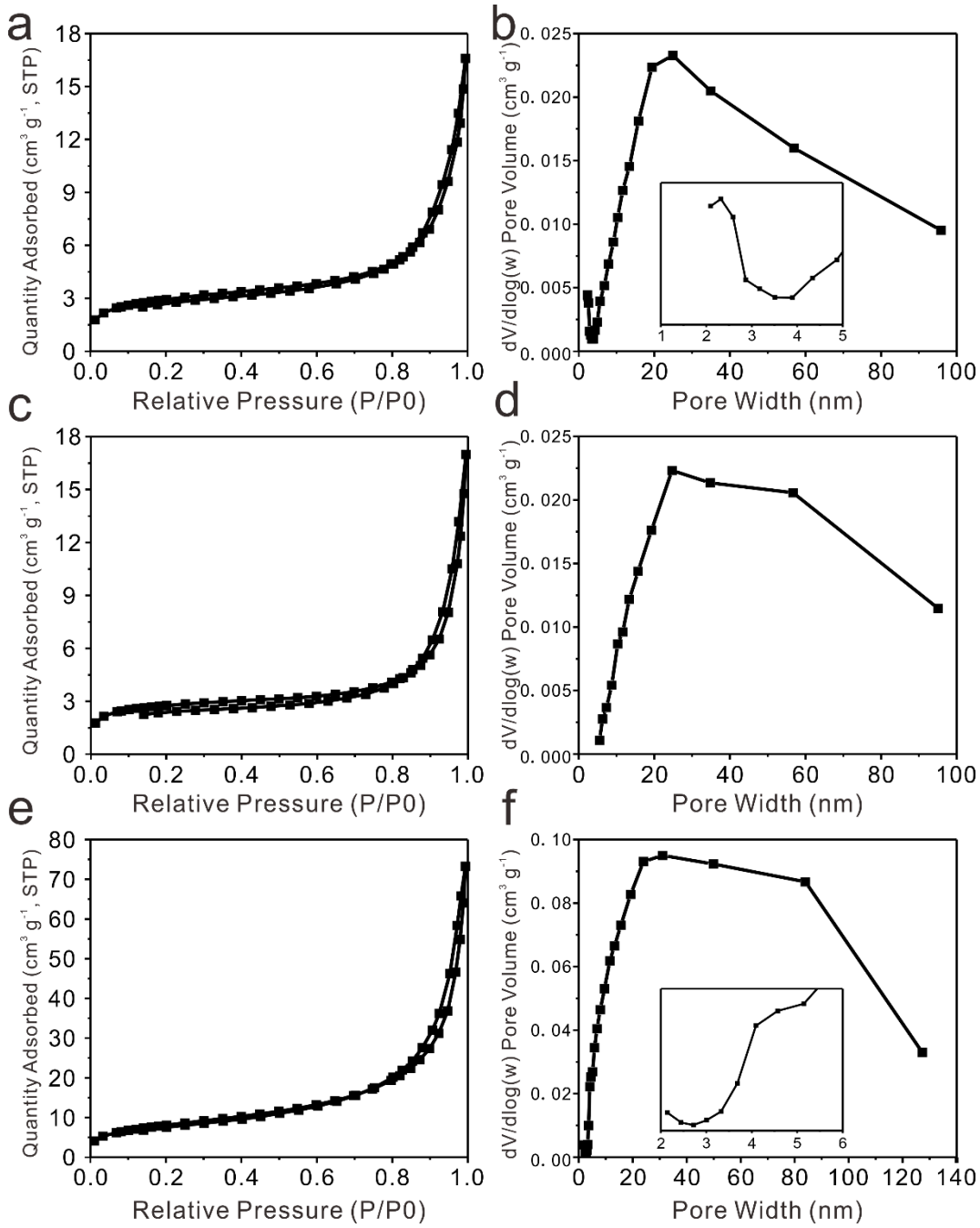

Figure S4. (a, c, e) Nitrogen adsorption and desorption isotherms of PBA, MPBA, and $FeCoS_x$-PBA. (b, d, f) pore size distribution of PBA, MPBA, and $FeCoS_x$-PBA.

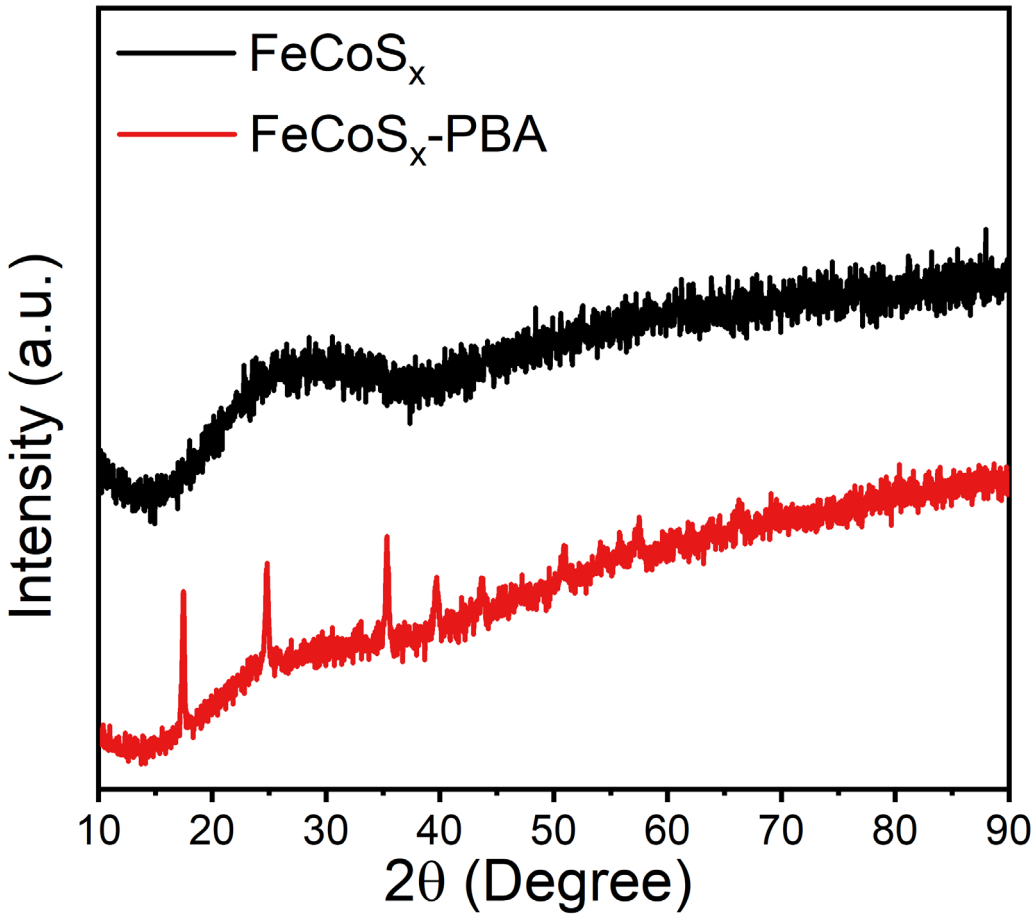

Figure S5. XRD spectra of $FeCoS_x$ and $FeCoS_x$-PBA.

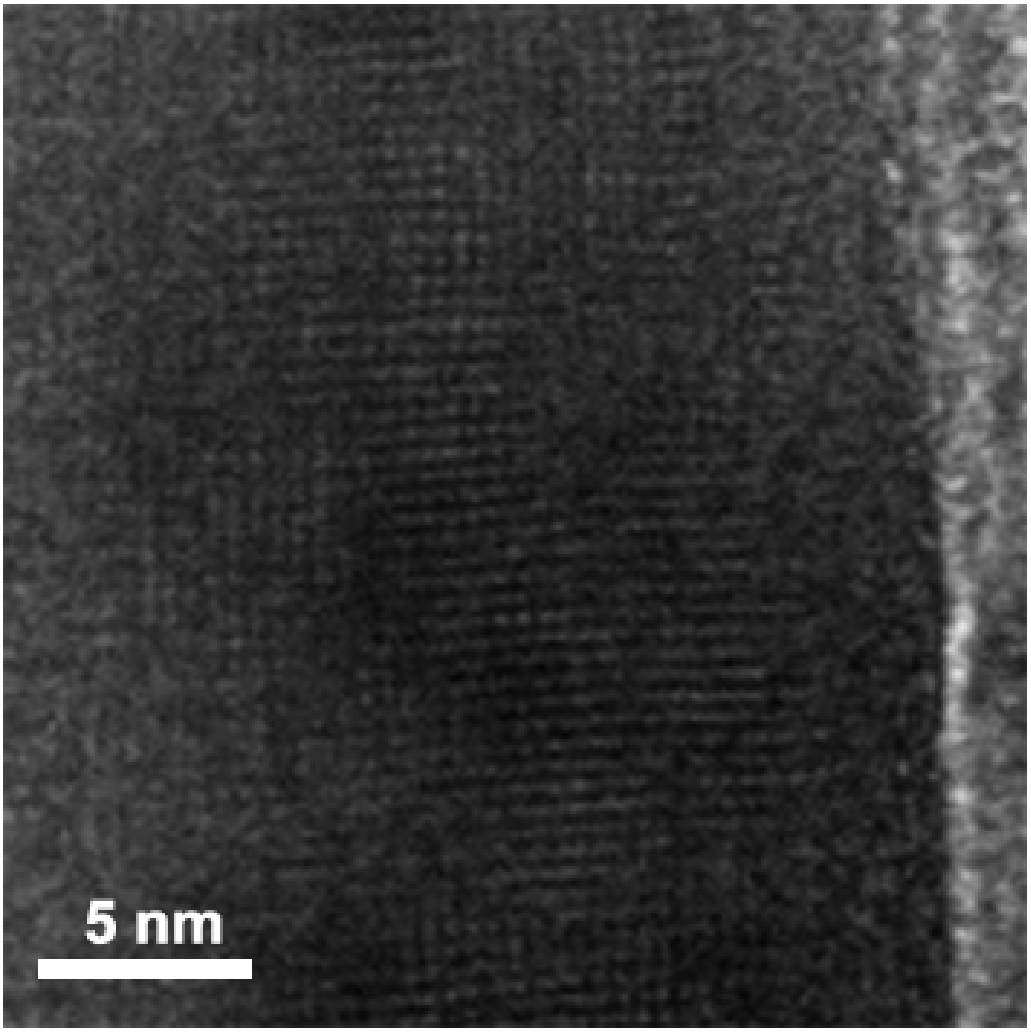

Figure S6. The original HRTEM image of $FeCoS_x$-PBA.

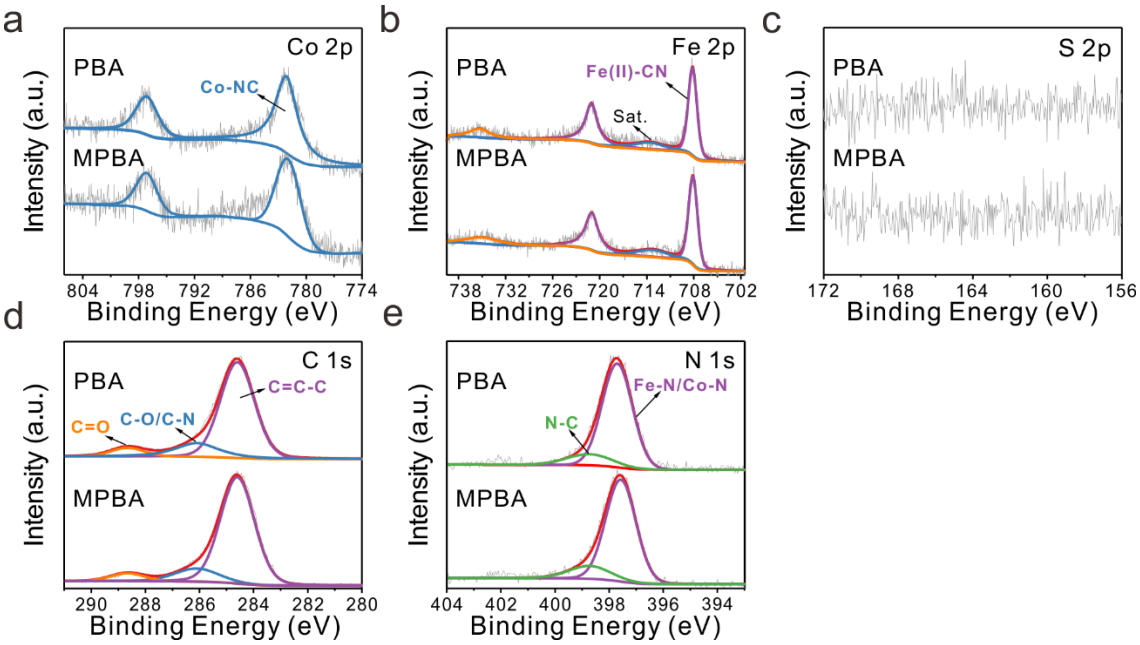

Figure S7. (a) Co 2p, (b) Fe 2p, (c) S 2p, (d) C 1s, (e) N 1s XPS spectra of PBA and MPBA.

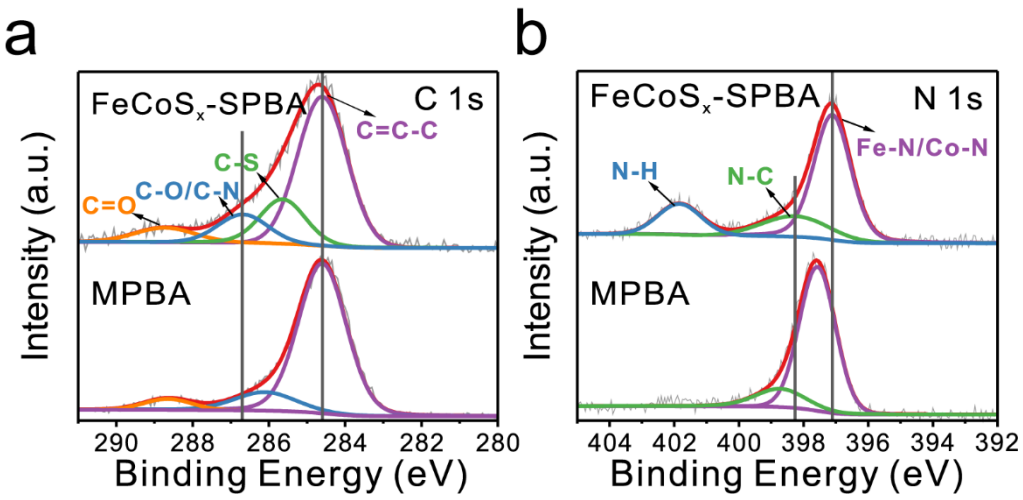

Figure S8. (a) C 1s, and (b) N 1s XPS spectra of $FeCoS_x$-PBA

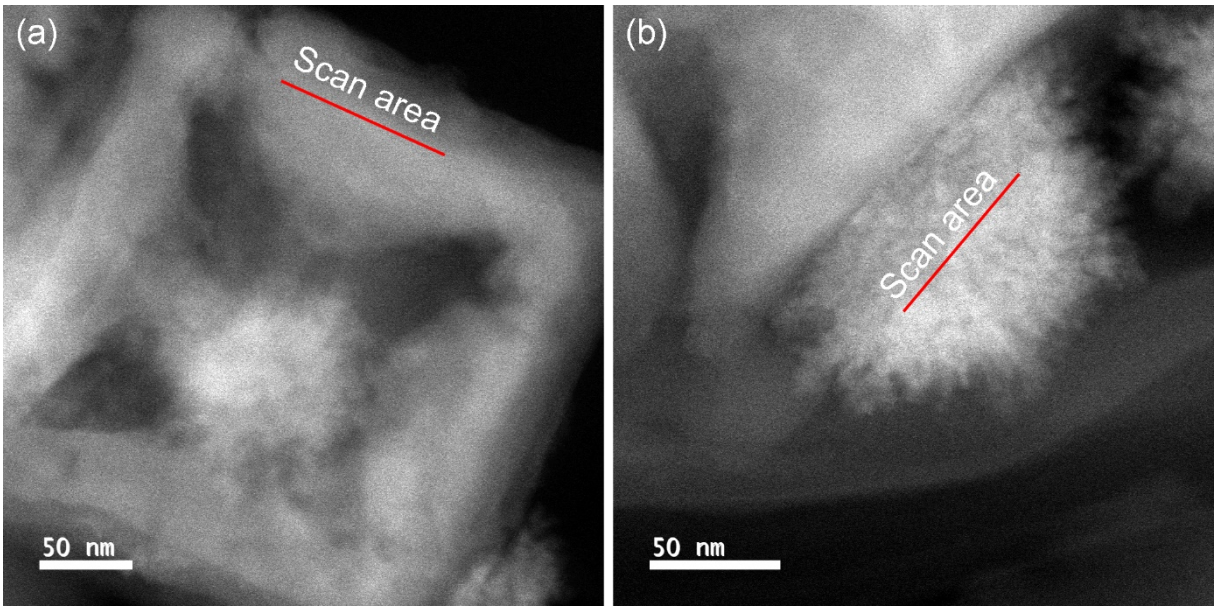

Figure S9. EELS scan area in $FeCoS_x$-PBA, (a) PBA frame, (b) amorphous $FeCoS_x$.

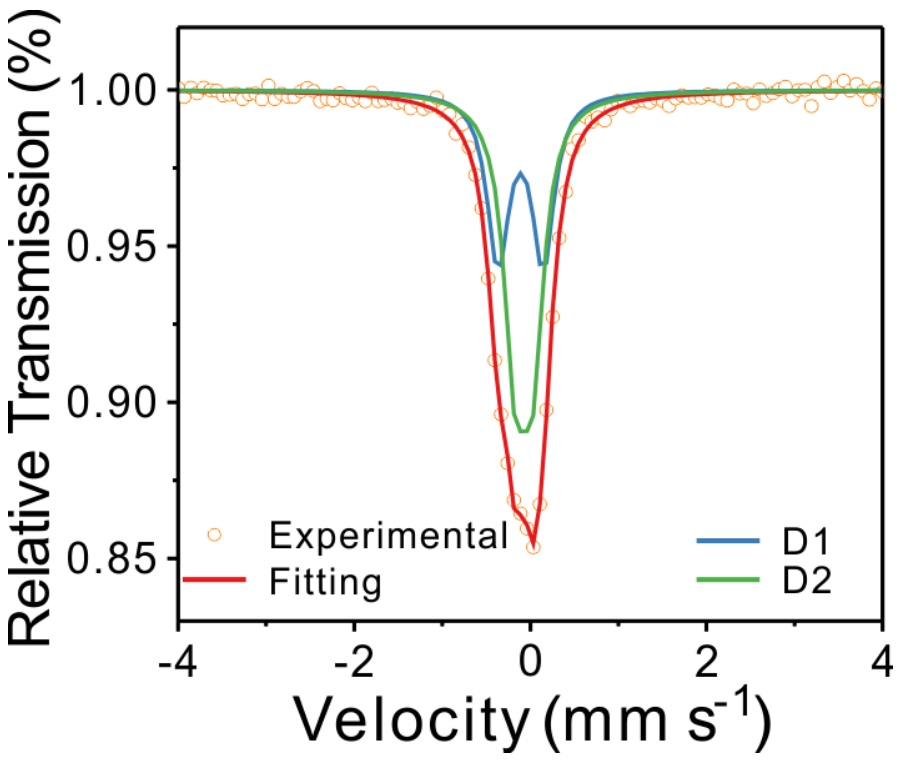

Figure S10. Mössbauer spectrum pattern of PBA.

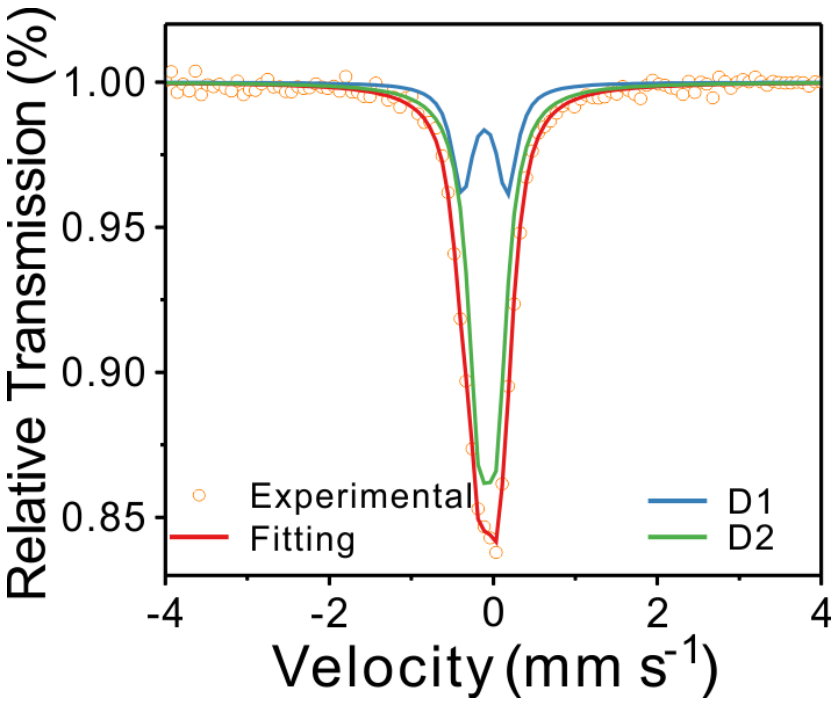

Figure S11. Mössbauer spectrum pattern of MPBA.

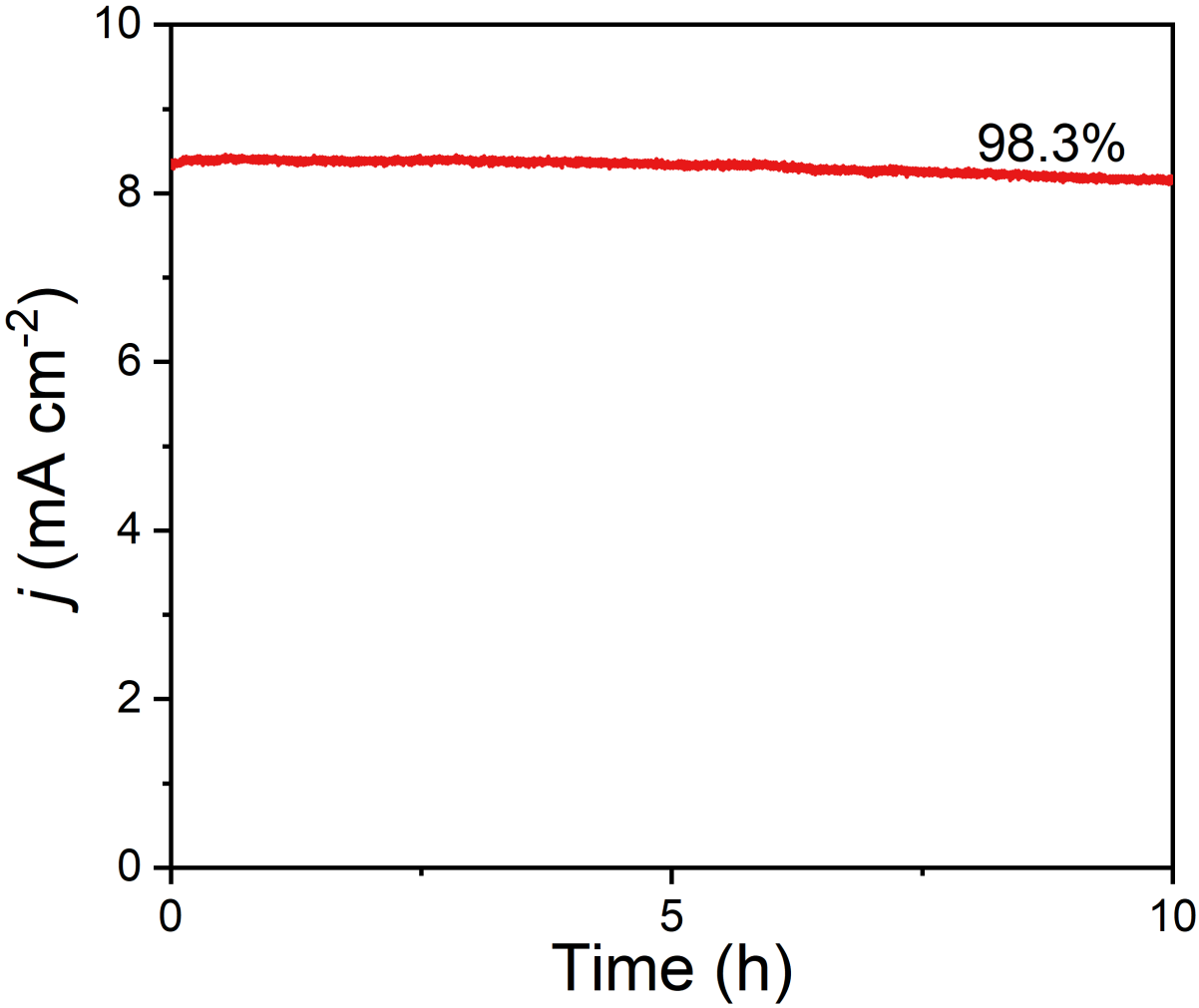

Figure S12. Chronoamperometric stability test of $FeCoS_x$-PBA.

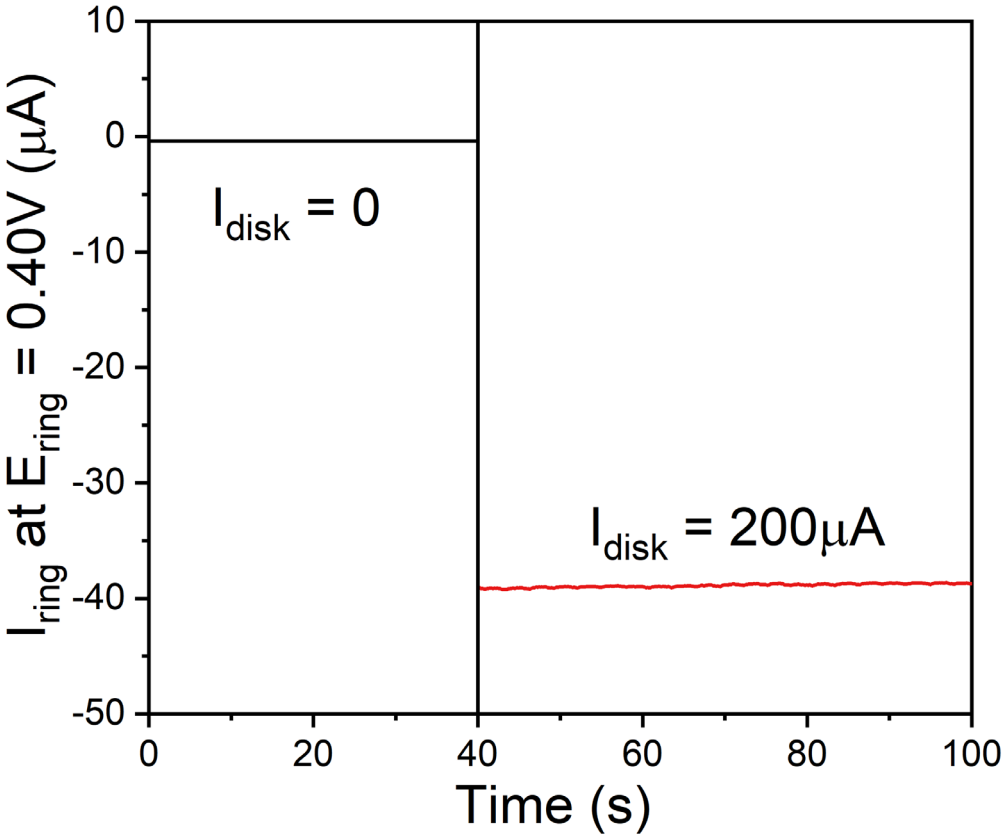

Figure S13. Faradic Efficency test, ring current of $FeCoS_x$-PBA on an RRDE (1600 rpm) in N_2-saturated 1 M KOH solution (ring potential 0.40 V).

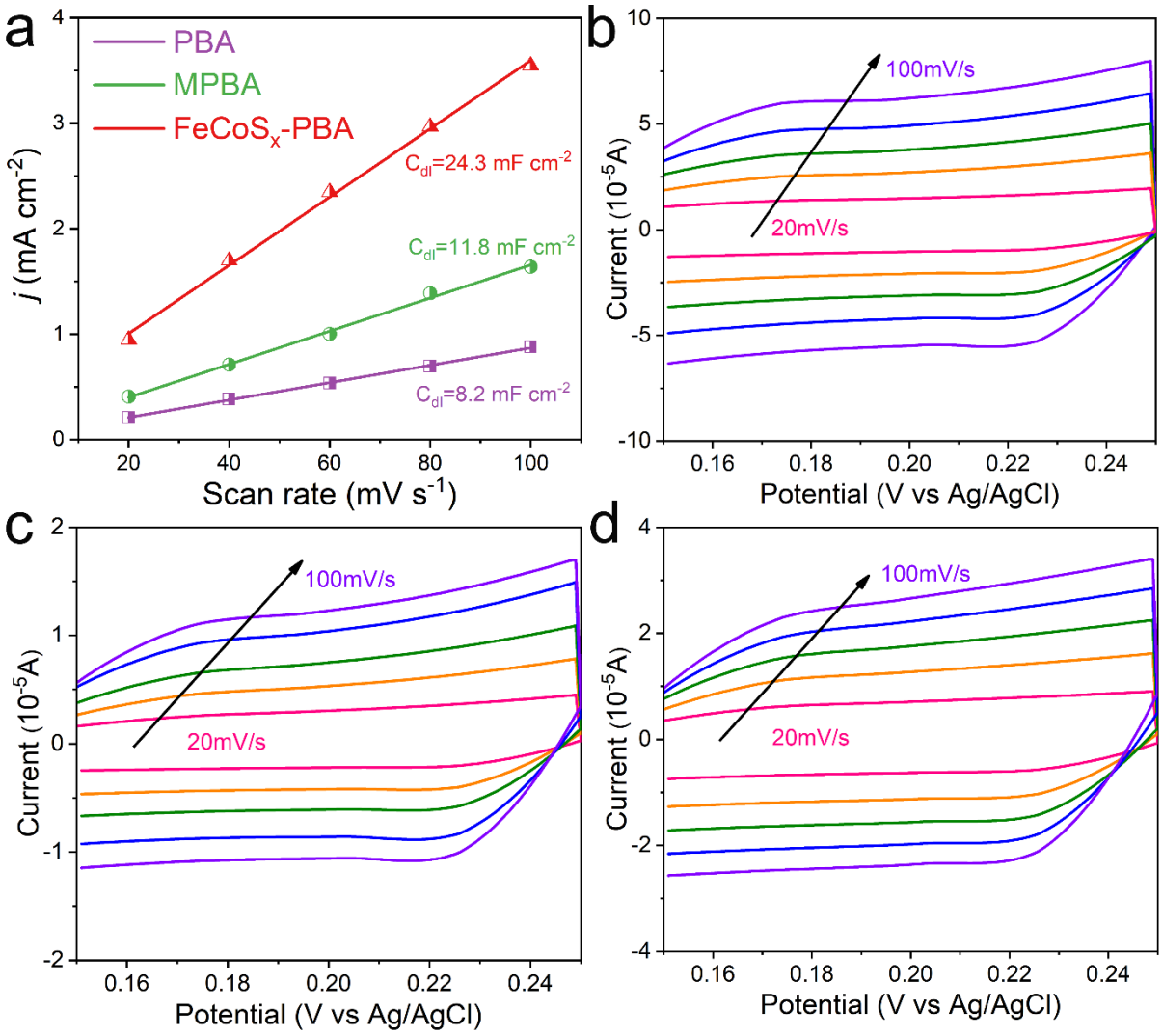

Figure S14. Electrochemical specific surface area test, (a) plots of the current density at 1.224 V vs the scan rate of PBA, MPBA and $FeCoS_x$-PBA. (b) Cyclic voltammetry data of PBA. (c) Cyclic voltammetry data of MPBA. (d) Cyclic voltammetry data of $FeCoS_x$-PBA.

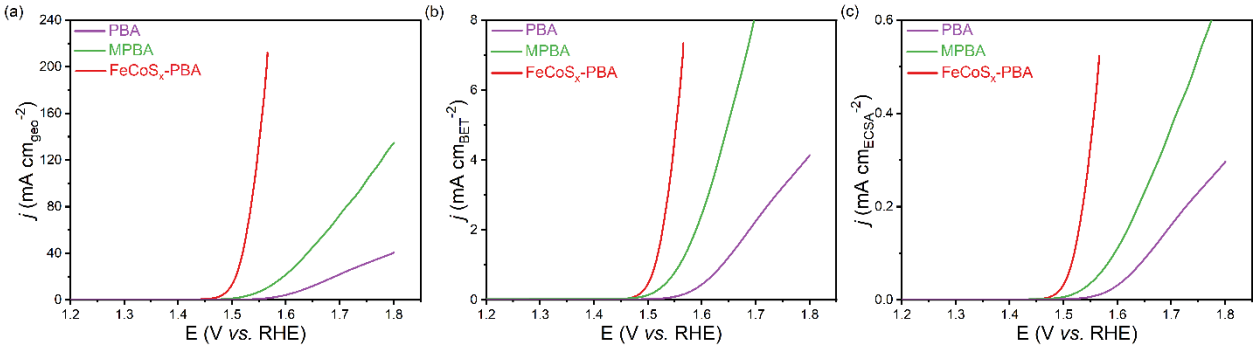

Figure S15. Polarization curves of PBA, MPBA, and $FeCoS_x$-PBA in an O_2-saturated 1 M KOH solution, the current is normalized by (a) electrode geometric area, (b) BET surface area, and (c) ECSA, respectively.

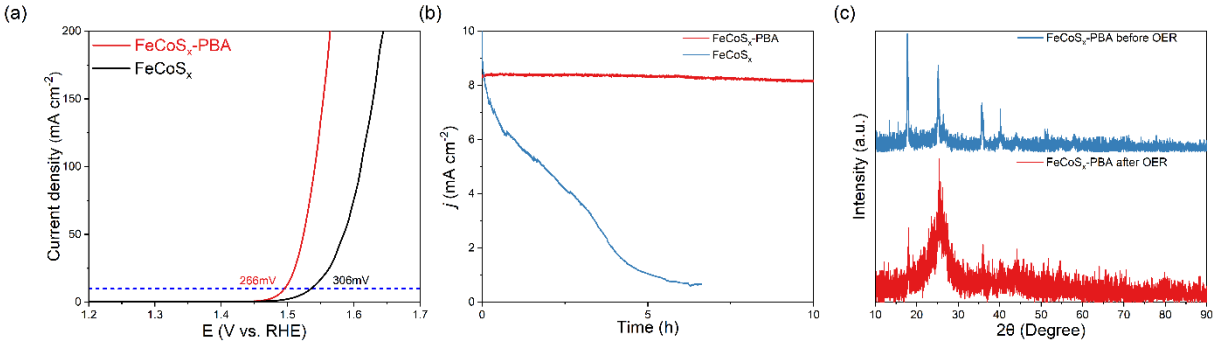

Figure S16. (a) Polarization curves and (b) chronoamperometric stability test of $FeCoS_x$ and $FeCoS_x$-PBA. (c) XRD pattern of $FeCoS_x$-PBA before and after OER test.

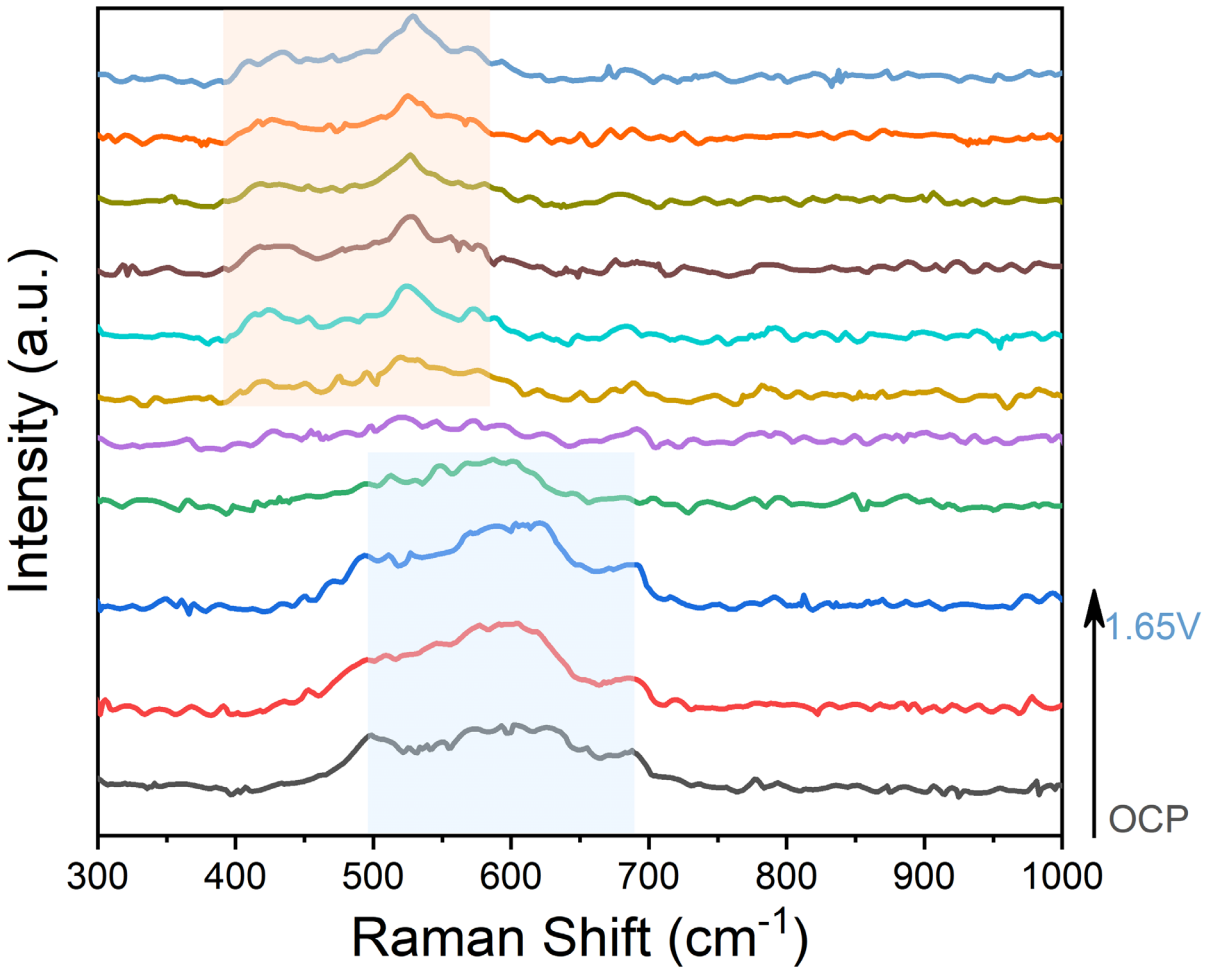

Figure S17. *In-situ* Raman spectrum of $FeCoS_x$-PBA.

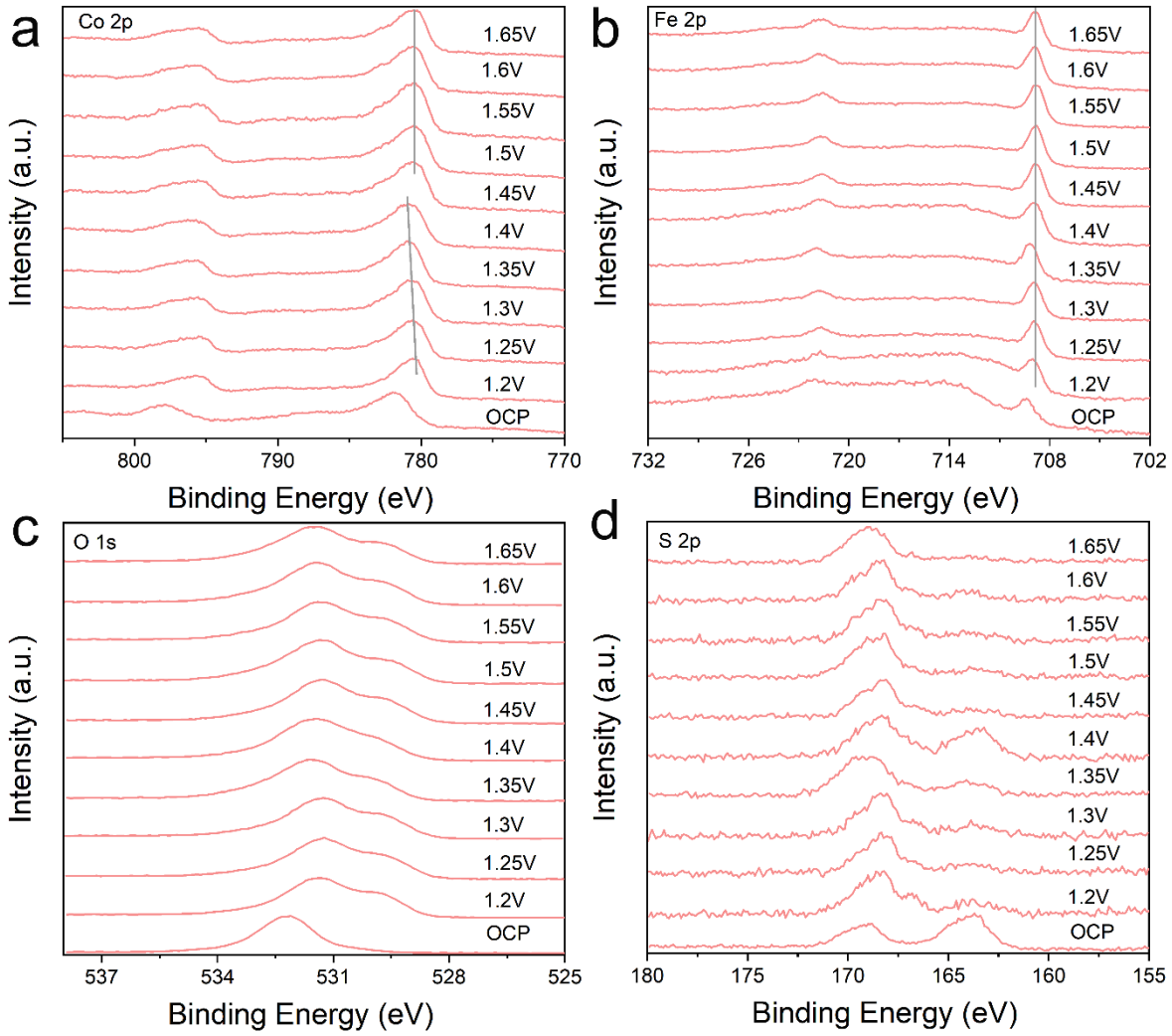

Figure S18. (a) Co 2p, (b) Fe 2p, (c) O 1s, (d) S 2p *quasi-in-situ* XPS spectrum of $FeCoS_x$-PBA.

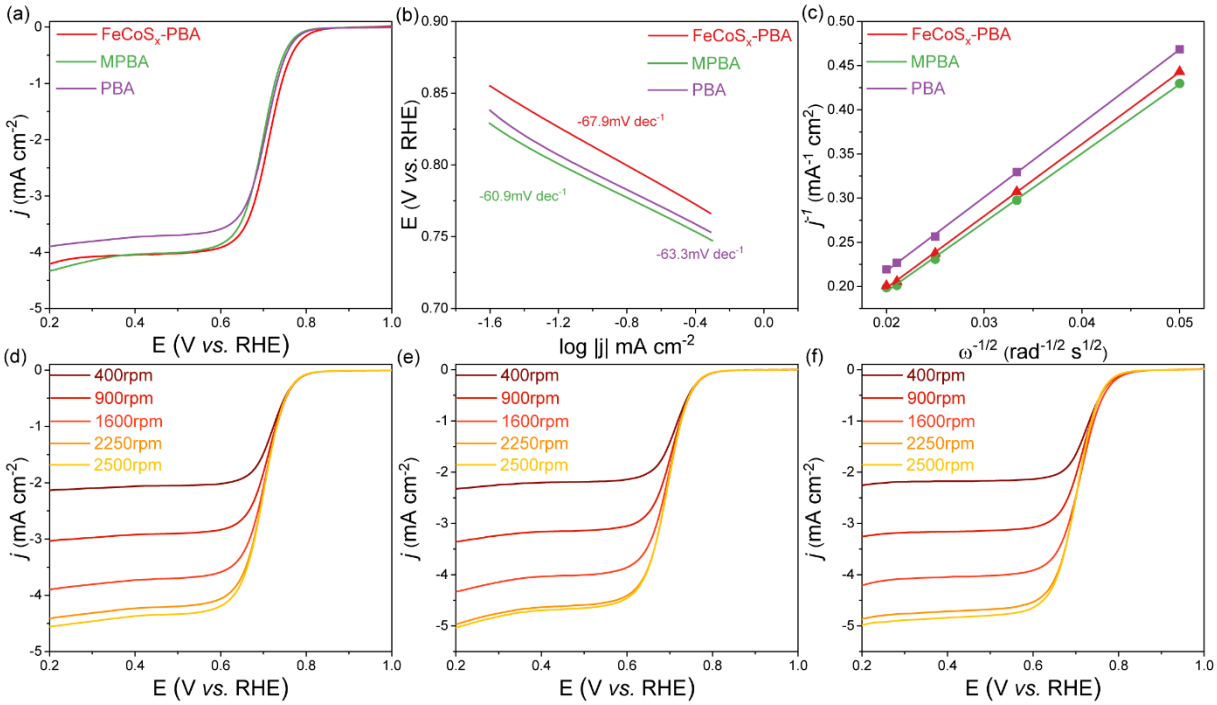

Figure S19. (a) ORR polarization curves of PBA, MPBA, and $FeCoS_x$-PBA at a rotation rate of 1600 rpm in O_2-saturated 1M KOH solution. (b) The Tafel plots of PBA, MPBA, and $FeCoS_x$-PBA. (c) Koutecky-Levich plots of PBA, MPBA, and $FeCoS_x$-PBA. The calculated electron transfer number are 3.2, 3.4, and 3.3, respectively. (d-f) Linear sweeping voltammetry curves at different rotation rate of (d) PBA, (e) MPBA, and (f) $FeCoS_x$-PBA.

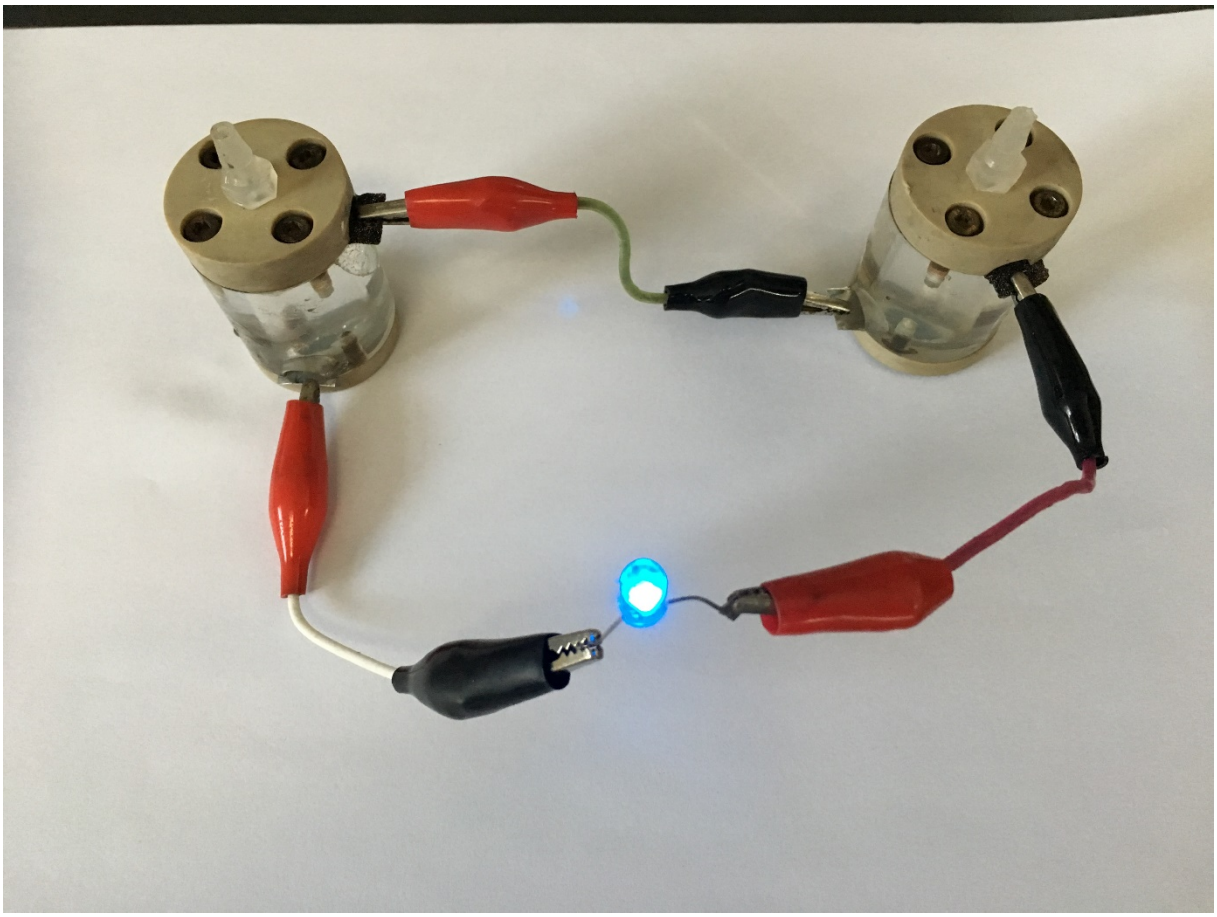

Figure S20. The blue light emitting diode (3.0 V) was lighted by two-series-connected Al-air batteries.

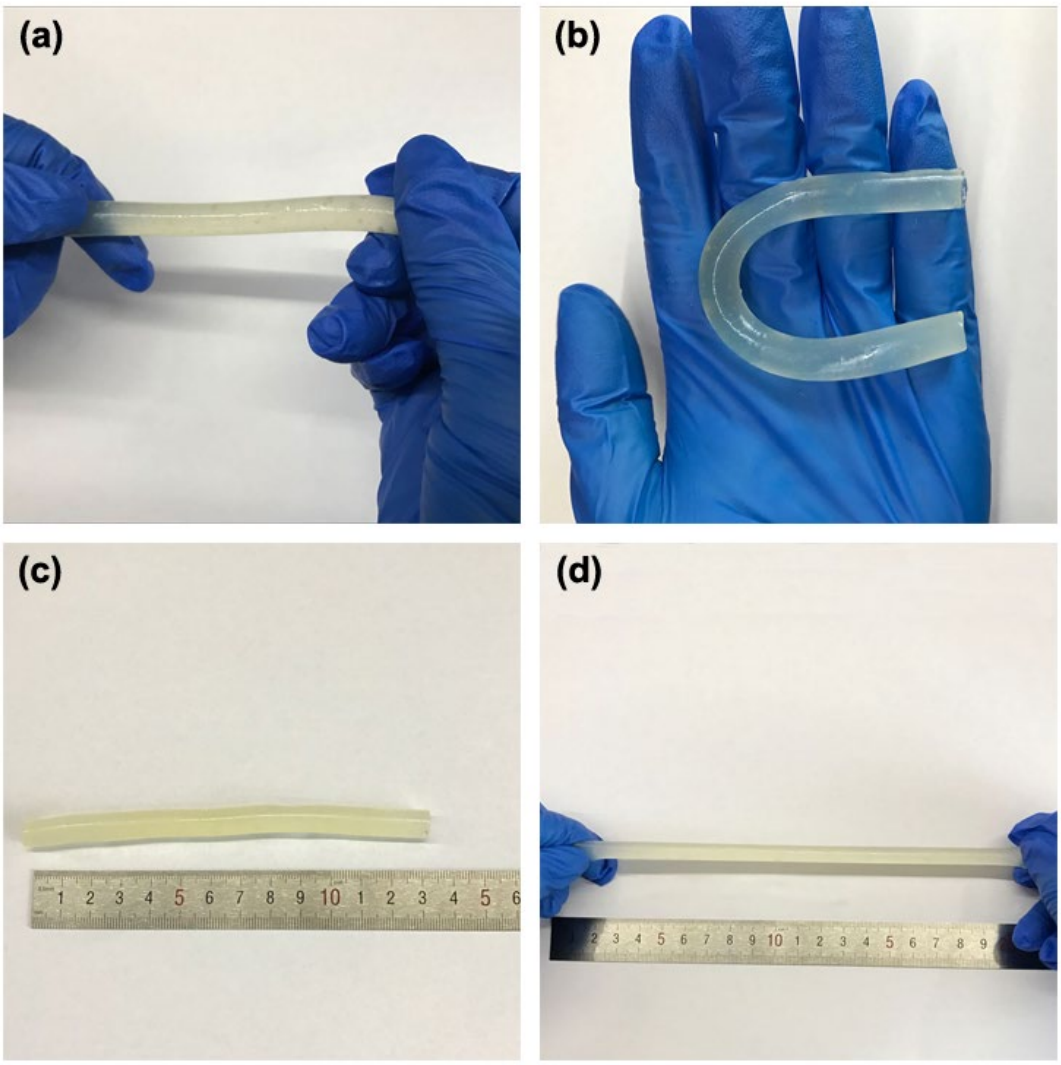

Figure S21. (a, b) Photographs of the fiber-like hydrogel electrolyte before and after bending, respectively. (c, d) Photographs of the fiber-like hydrogel electrolyte before and after stretching, respectively.

Table S1. Textural properties of as-prepared materials.

Catalysts	Specific surface area [m^2 g^{-1}]	Pore volume [cm^3 g^{-1}]	Pore diameter [nm]
PBA	9.7834	0.024556	18.1548
MPBA	8.8872	0.024941	27.4943
$FeCoS_x$-PBA	28.9122	0.115007	18.2307

Table S2. ^{57}Fe Mössbauer parameters of PBA, MPBA, and $FeCoS_x$-PBA derived from the fittings. Isomer shift (IS), quadrupole splitting (QS), line width (LW) and relative spectral area % of each component.

Component	IS [mm s^{-1}]	QS [mm s^{-1}]	LW [mm s^{-1}]	Aera [%]
PBA-D1	-0.11	0.52	0.29	40.6
PBA-D2	-0.07	0.20	0.30	59.4
MPBA-D1	-0.11	0.55	0.29	25.6
MPBA-D2	-0.07	0.21	0.32	74.4
$FeCoS_x$-PBA-D1	0.01	0.15	0.30	55.9
$FeCoS_x$-PBA-D2	0.23	0.78	0.33	44.1

Table S3. Comparison of OER electrocatalytic activities for $FeCoS_x$-PBA with other catalysts.

Catalysts	Overpotential at j =10 mA cm^{-2} [mV]	Tafel slope [mV dec^{-1}]	*Ref.*
$FeCoS_x$-PBA	**266**	**33**	**This work**
Co_9S_8	265	56	1
Co_8FeS_8/CoS	292	83	2
Co_3O_4	253	74.6	3
$Ni_{0.85}Fe_{0.15}PS$	251	34	4
Co_9S_8/CoS_2	396	182	5
$Fe_{0.1}Ni_{0.9}S_2$	260	46	6
$CoSe_2$	320	44	7
NiCoP-C	320	96	8

Table S4. The performance of Al-air batteries with various electrocatalys.

Catalysts	Loading [mg cm^{-2}]	Peak power density [mW cm^{-2}]	Specific capacity [mAh g^{-1}]	Energy density [Wh Kg^{-1}]	*Ref.*
$FeCoS_x$-PBA	**2**	**58.3**	**1259**	**1483**	**This work**
Ag-coated CNT	0.0669	1.33	935	1168	9
$La_{0.6}Ca_{0.4}CoO_3$	-	16	458	641	10
MnO_x/carbon fiber	-	5.5	105	176.4	11
$LiMn_2O_4$/N-rGO	1.5	6.6	585	673	12
Carbon black	0.43	3	496	267.8	13
CoO	-	48	523.6	451.1	14
N-rGO	1.5	7	254.6	130	15
60% Pt/C	2	83	74	92	16
N,S-porous carbon	0.5	46	288	273	17
CoP@N,P-CNFs	-	72.8	2824.3	-	18
3D nanoporous N-doped carbon	0.5	130.5	-	-	19

References

[1] H. Zhang, J. Wang, Q. Cheng, P. Saha, H. Jiang, *Green Energy & Environ.* 2020, **5**, 492.

[2] B. Wang, Y. Chen, X. Wang, X. Zhang, Y. Hu, B. Yu, D. Yang, W. Zhang, *J. Power Sources.* 2020, **449**, 227561.

[3] B. Jin, Y. Li, J. Wang, F. Meng, S. Cao, B. He, S. Jia, Y. Wang, Z. Li, X. Liu, *Small.* 2019, **15**, 1903847.

[4] W. Peng, J. Li, K. Shen, L. Zheng, H. Tang, Y. Gong, J. Zhou, N. Chen, S. Zhao, M. Chen, F. Gao, H. Gou, *J. Mater. Chem. A.* 2020, **8**, 23580.

[5] Y. Dong, J. Ran, Q. Liu, G. Zhang, X. Jiang, D. Gao, *RSC Adv.* 2021, **11**, 30448.

[6] X. Ding, W. Li, H. Kuang, M. Qu, M. Cui, C. Zhao, D.-C. Qi, F. E. Oropeza, K. H. L. Zhang, *Nanoscale.* 2019, **11**, 23217.

[7] Y. Liu, H. Cheng, M. Lyu, S. Fan, Q. Liu, W. Zhang, Y. Zhi, C. Wang, C. Xiao, S. Wei, B. Ye, Y. Xie, *J. Am. Chem. Soc.* 2014, **136**, 15670.

[8] P. He, X. Y. Yu, X. W. Lou, *Angew. Chem. Int. Ed.* 2017, **129**, 3955.

[9] Y. Xu, Y. Zhao, J. Ren, Y. Zhang, H. Peng, *Angew. Chem. Int. Ed.* 2016, **128**, 8111.

[10] C. Li, W. Ji, J. Chen, Z. Tao, *Chem. Mater.* 2007, **19**, 5812.

[11] A. A. Mohamad, *Corros. Sci.* 2008, **50**, 3475.

[12] Y. Liu, J. Li, W. Li, Y. Li, Q. Chen, Y. Liu, Int. *J. Hydrogen. Energ.* 2015, **40**, 9225.

[13] S. Choi, D. Lee, G. Kim, Y. Y. Lee, B. Kim, J. Moon, W. Shim, *Adv. Funct. Mater.* 2017, **27**, 1702244.

[14] I. J. Park, S. R. Choi, J. G. Kim, *J. Power. Sources.* 2017, **357**, 47.

[15] Y. Liu, J. Li, W. Li, Y. Li, F. Zhan, H. Tang, Q. Chen, *Int. J. Hydrogen. Energ.* 2016, **41**, 10354.

[16] L. Wang, F. Liu, W. Wang, G. Yang, D. Zheng, Z. Wub, M. K. H. Leungc, *RSC Adv.* 2014, **4**, 30857.

[17] L. Xu, H. Fan, L. Huang, J. Xia, S. Li, M. Li, H. Ding, K. Huang, *Electrochim. Acta.* 2017, **239**, 1.

[18] J. Liu, C. Zhang, S. Yuan, W. Yang, Y. Cao, J. Deng, B. Xu, H. Lu, *Chem. Eng. J.* 2022, **428**, 131326.

[19] K. Hu, T. Yu, Y. Zhang, X. Lin, Y. Zhao, G. Xie, X. Liu, X. Lin, J. Fujita, H.-J. Qiu, Y. Ito, *Adv. Funct. Mater.* 2021, **31**, 2103632.